



Cite this: *Analyst*, 2022, **147**, 4433

## Reusable and universal impedimetric sensing platform for the rapid and sensitive detection of pathogenic bacteria based on bacteria-imprinted polythiophene film<sup>†</sup>

Lingling Wang,<sup>‡,a</sup> Xiaohui Lin,<sup>‡,a</sup> Ting Liu,<sup>a</sup> Zhaohuan Zhang,<sup>a</sup> Jie Kong,<sup>a</sup> Hai Yu,<sup>a</sup> Juan Yan,<sup>‡,a</sup> Donglei Luan,<sup>a</sup> Yong Zhao<sup>\*,a</sup> and Xiaojun Bian<sup>‡,a,b,c</sup>

The rapid and sensitive detection of pathogenic bacteria is highly demanded for early warning of infectious disease epidemics and protection of human health. Herein, a reusable and universal impedimetric sensing platform based on a bacteria-imprinted polythiophene film (BIF) is proposed for the rapid and sensitive detection of pathogenic bacteria using *Staphylococcus aureus* (*S. aureus*) as a model analyte. Monomer screening among four 3-substituted thiophenes was first performed based on the imprinting factor, and 3-thiopheneethanol (TE) was eventually selected. The BIF as a recognition layer was quickly deposited in an environmentally friendly process on a glassy carbon electrode via electro-copolymerization of the *S. aureus* template and TE monomer followed by *in situ* template removal. Upon rebinding of *S. aureus* on the BIF, the impedance increased. Under optimal conditions, the BIF-based sensor can quantitatively detect *S. aureus* in a wide linear range of 10 to  $10^7$  CFU mL<sup>-1</sup> with a low detection limit of 4 CFU mL<sup>-1</sup>. Additionally, the sensor exhibits excellent selectivity, capable of identifying *S. aureus* from multi-bacterial strain mixtures. It also demonstrates applicability in the analysis of real lettuce and shrimp samples with good recoveries. Most significantly, the BIF sensing interface can be reused up to five times with good signal retention. Compared with most reported methods, this sensor is more rapid with a much shorter total assay time of 30 min, including the BIF preparation, bacterial rebinding, and impedance detection. This assay may hold great potential to help in the rapid, sensitive, and label-free detection of pathogenic bacteria in fields of food safety and public health.

Received 12th July 2022,  
Accepted 12th August 2022

DOI: 10.1039/d2an01122k

rsc.li/analyst

## Introduction

Pathogenic bacterial infections represent leading causes of hospitalizations and deaths in both developed and developing countries, taking more than 6.7 million lives each year.<sup>1</sup> Among the various bacterial strains, *Staphylococcus aureus* (*S. aureus*) is one of the most dangerous human pathogens responsible for many diseases ranging from mild skin and soft tissue infections, food poisoning to serious or even life-threatening diseases including bacteremia, sepsis, pneumonia,

endocarditis, osteomyelitis, and toxic shock syndrome.<sup>2,3</sup> Moreover, *S. aureus* can rapidly adapt to antibiotics and evolve into antibiotic-resistant bacteria, such as methicillin-resistant *S. aureus* (MRSA), that have imposed huge burdens on medical care, and posed serious threats to human life.<sup>4,5</sup> Existing methods for tracking pathogenic bacteria such as cell culturing,<sup>6</sup> enzyme-linked immunosorbent assay (ELISA),<sup>7,8</sup> polymerase chain reaction (PCR),<sup>9,10</sup> mass spectrometry,<sup>11,12</sup> flow cytometry,<sup>13</sup> and surface-enhanced Raman scattering (SERS)<sup>14,15</sup> are accurate and reliable. Still, they are restricted by lengthy analysis times, insufficient sensitivity, complicated operation, or expensive instruments and reagents. Therefore, rapid, sensitive, simple, and low-cost methods for detecting pathogenic bacteria are still highly demanded.

Electrochemical sensors have received considerable attention for pathogen detection due to their fast response, easy operation, low cost, and portability.<sup>16</sup> Moreover, electrochemical sensors are robust due to their direct and label-free detection of whole bacterial cells without tedious processes, including cell lysis, nucleic acid extraction, and signal amplifi-

<sup>a</sup>College of Food Science and Technology, Shanghai Ocean University, Shanghai 201306, China. E-mail: yzhao@shou.edu.cn, xjbian@shou.edu.cn; Fax: +86-21-61900753; Tel: +86-21-61900753

<sup>b</sup>Laboratory of Quality and Safety Risk Assessment for Aquatic Product on Storage and Preservation (Shanghai), Ministry of Agriculture, Shanghai 201306, China

<sup>c</sup>Shanghai Engineering Research Center of Aquatic-Product Processing & Preservation, Shanghai 201306, China

<sup>†</sup> Electronic supplementary information (ESI) available. See DOI: <https://doi.org/10.1039/d2an01122k>

<sup>‡</sup>These authors have equally contributed to this article.

cation. The most crucial aspect in the construction of label-free electrochemical sensors for the detection of pathogenic bacteria is the choice of suitable recognition elements and their efficient immobilization onto the electrode surface. Among various recognition elements (e.g., antibodies,<sup>4,17</sup> aptamers,<sup>18–20</sup> antimicrobial peptides,<sup>21</sup> etc.), antibodies are the most commonly used due to their high selectivity and binding affinity. However, antibodies are limited by their drawbacks of requiring animals for production, high cost, and low tolerance to harsh conditions such as high temperatures and salt concentrations, strong acids or bases, and organic solvents. Besides, antibodies may suffer from conformational changes or denaturation when being immobilized on the transducer surface through adsorption or covalent coupling.<sup>22</sup>

Molecularly imprinted polymers (MIPs) are synthetic antibody mimics with tailor-made binding sites complementary in physical (shape and size) and chemical (structure and functionality) features to that of a template.<sup>23</sup> MIPs have many distinct advantages, such as easy preparation, being cost-efficient, and having long-term physical and chemical stability, which make them promising alternatives to natural antibodies.<sup>24</sup> Owing to these unique characteristics, MIPs have been integrated with various sensing platforms for detecting simple organic molecules,<sup>25–27</sup> and biomacromolecules like proteins,<sup>28,29</sup> viruses,<sup>30</sup> and bacteria.<sup>31</sup> However, we have to acknowledge that the imprinting of whole bacterial cells is still very challenging due to their large size and complex chemical composition, leading to increased difficulty in the complete removal of the template, and the generation of imprinted sites with good accessibility and recognition capability.<sup>32</sup>

To overcome the difficulties mentioned above, various surface imprinting strategies such as stamping/microcontact,<sup>33</sup> Pickering emulsion polymerization,<sup>34</sup> colloidal imprinting,<sup>35,36</sup> and electro-polymerization<sup>37</sup> have been proposed. However, most of these are cumbersome, time-consuming, and environmentally unfriendly, using large amounts of toxic reagents such as cross-linkers, initiators, and organic solvents. In comparison, electro-polymerization offers a simple, fast, and green method for the direct synthesis of MIP films *in situ* on the electrode surface, avoiding the use of cross-linkers and initiators.<sup>38</sup> By varying the electro-polymerization parameters, the thickness of polymer films can be easily controlled, and thus it is conducive to better template removal and site accessibility. Moreover, electropolymerized MIPs (e-MIPs) can be facilely integrated with an electrochemical sensing platform, omitting the step of electrode modification.<sup>25</sup>

Though synthesizing e-MIPs is a simple process, the construction of e-MIPs-based electrochemical bacterial sensors with a desired sensing performance (rapidity, sensitivity, selectivity, and simplicity) remains a challenge. One critical solution to tackling this challenge is the selection of suitable functional monomers that provide good interactions with bacterial cells (template).<sup>39,40</sup> Since the chemical composition of the bacterial surface is complex, it is difficult to build specific covalent bindings for template-monomers, and thus noncovalent interactions such as hydrogen bonding are preferred.<sup>41</sup>

Herein, a universal and regenerable impedimetric sensor based on an electropolymerized bacteria-imprinted polythiophene film (BIF) was proposed for the rapid, sensitive, and label-free detection of pathogenic bacteria using *S. aureus* as a model analyte. Considering the existence of various functional groups (hydroxyl, carboxyl, phosphoryl, and amide) on the bacterial surface,<sup>42</sup> four 3-substituted thiophenes, including 3-thiopheneacetic acid (TAA), 3-thiopheneboronic acid (TBA), 3-thiophenemethylamine (TMA), and 3-thiopheneethanol (TE), were selected as potential functional monomers for the electro-synthesis of four different BIFs. As shown in Scheme 1, the BIF was *in situ* formed on a glassy carbon electrode (GCE) via the cyclic voltammetric electro-copolymerization of each monomer and the *S. aureus* template in phosphate buffer solution (PBS) followed by template removal. The BIF preparation is speedy, green, and low cost, and can be finished within 15 min without using any harmful organic solvents. After the recognition of the target *S. aureus* within 10 min, the electron transfer between the  $[\text{Fe}(\text{CN})_6]^{3-/-4-}$  redox couple and GCE were blocked, leading to an increase in the BIF impedance, detected by electrochemical impedance spectroscopy (EIS). By comparing the imprinting factor of the four monomers, TE was eventually used to construct the BIF-based impedimetric sensor. Compared with most existing methods, this sensor is more sensitive and rapid with a lower limit of detection (LOD), and a much shorter total assay time. Moreover, the sensing interface can be regenerated and reused at least five times. Additionally, the applicability of the sensor was also evaluated using real lettuce and shrimp samples. The proposed assay could provide a universal and straightforward method for the rapid, sensitive, and highly selective detection of pathogenic bacteria.

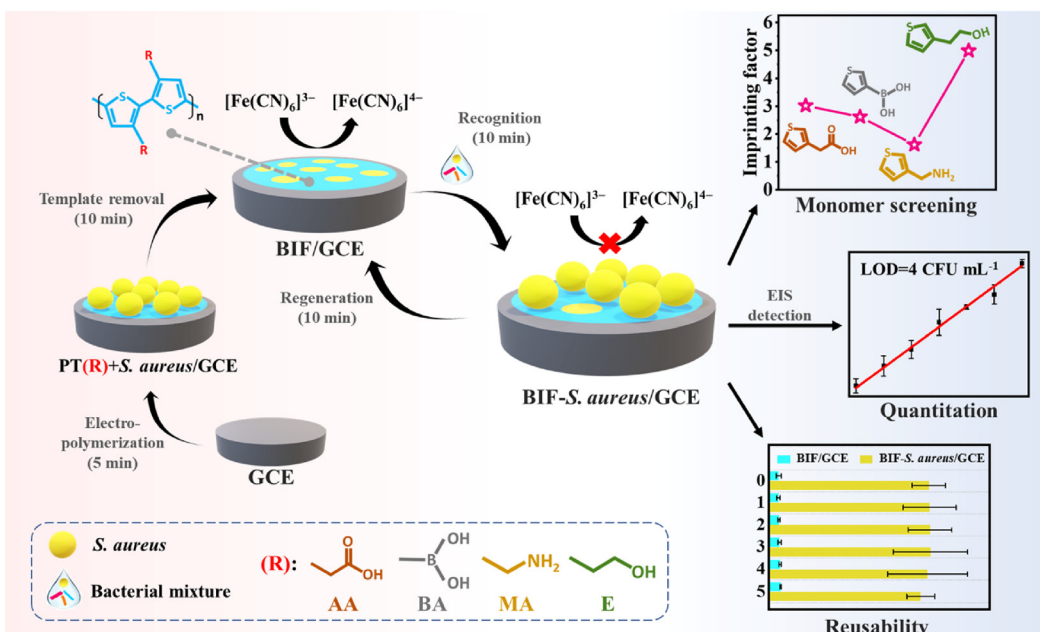
## Experimental section

### Preparation of bacteria

The pure isolates of *S. aureus* (ATCC 25923), *Listeria monocytogenes* (*L. monocytogenes*, ATCC 19115), *Escherichia coli* O157:H7 (*E. coli* O157, ATCC 43889), and *Salmonella Paratyphi* B (*S. Paratyphi* B, CMCC 50094) were involved in the experiment. All the bacterial strains were separately grown overnight in a liquid medium at 37 °C with continuous shaking at 200 rpm, and then were quantified by the plate count method. Afterward, the bacterial culture was fixed with 100-fold diluted formaldehyde (37–40% in water). Such formaldehyde inactivated bacteria were used during the whole experiment.

### Electrochemical measurements

Electrochemical measurements were carried out using a CHI 660E workstation with a standard three-electrode system. A GCE (3 mm in diameter), platinum sheet electrode, and saturated calomel electrode (SCE) served as working, auxiliary, and reference electrodes, respectively. EIS of differently modified GCEs were recorded in 0.1 M KCl containing 1 mM  $[\text{Fe}(\text{CN})_6]^{3-/-4-}$  redox couple, using an open circuit voltage over a frequency range of 0.1–100 000 Hz with an amplitude of



**Scheme 1** Schematic illustration of constructing a regenerable bacteria imprinted polythiophene film (BIF)-based impedimetric sensor for the rapid, sensitive, and label-free detection of *S. aureus*.

5 mV. Cyclic voltammetry (CV) measurements were performed in 0.1 M KCl containing 5 mM [Fe(CN)<sub>6</sub>]<sup>3-</sup>.

### BIF preparation

A polished GCE was immersed in 5 mL PBS (0.1 M, pH 6.5) containing one of the four monomers (8 mM) and the *S. aureus* template ( $10^9$  CFU mL<sup>-1</sup>), and CV was performed under mild stirring for 10 cycles at a scan rate of 0.1 V s<sup>-1</sup>. CV electro-polymerizations in the presence of different monomers were carried out under the same conditions except for the potential sweep range. For TE and TMA, the potential scanning was started from -0.6 to 1.0 V, while for TAA and TBA, the potential scanning range was -0.5–1.0 V, and -0.2–1.2 V, respectively. The modified electrode formed through electro-copolymerization was denoted as PT(R) + *S. aureus*/GCE, as shown in Scheme 1, where (R) represents the shortened form of the side chain group of each monomer. To elute the template bacteria, the PT(R) + *S. aureus*/GCE was soaked in CTAB (1 mM) dispersed in a diluted acetic acid solution (36%, v/v), referred to as CTAB/HAc, at 37 °C for 10 min under constant shaking (400 rpm). Such a prepared modified electrode was named BIF/GCE. As a control, a non-imprinted polythiophene film (NIF) modified electrode (NIF/GCE) was prepared *via* the same procedure as that of the corresponding BIF/GCE, but excluding the template bacteria from the polymerization solution.

### Fluorescence imaging

The target *S. aureus* cells ( $10^5$  CFU mL<sup>-1</sup>) were stained with SYTO 9 green fluorescent dye (Invitrogen) according to the manufacturer's instructions. Detachable GCEs (Gaoss Union,

China; 3 mm in diameter) were used for the formation of BIF/GCE and NIF/GCE that were separately incubated with stained *S. aureus* under dark conditions for 10 min. The fluorescence imaging was *in situ* observed on the electrode surface using a fluorescence microscope (DP80, Olympus) through an optical filter with an excitation of 460–480 nm and an emission of 495–540 nm.

### Electrochemical detection of *S. aureus*

The freshly prepared BIF/GCE was incubated with different concentrations of *S. aureus* in PBS (0.01 M, pH 7.4) at 37 °C for 10 min under constant shaking (250 rpm). The resulting electrode (marked as BIF-*S. aureus*/GCE) was rinsed with water and dried in a N<sub>2</sub> atmosphere for immediate EIS measurements. To minimize the variability between electrodes in parallel, the EIS response of BIF/GCE towards target bacteria was described by the relative variation of the charge transfer resistance ( $R_{ct}$ ),  $[\Delta R/R(\Omega)]$ .<sup>43</sup> The value was calculated using the following formula:

$$\Delta R/R = (R_{cta} - R_{ctb})/R_{ctb} \quad (1)$$

where  $R_{ctb}$  and  $R_{cta}$  represent the value of  $R_{ct}$  before and after capturing the target bacteria, respectively.

### Optimization of experimental conditions

To obtain the optimal sensing performance, six experimental conditions, including polymerization cycles (5–15), template concentration ( $10^7$ – $10^9$  CFU mL<sup>-1</sup>), template elution (types of eluents and elution time from 5–15 min), recognition time (5–15 min), and oscillation speed during recognition (0–300 rpm) were optimized independently. The choice of the

optimum experimental conditions, except template elution dependent on the degree of reduction in the  $R_{ct}$  value, was based on the  $\Delta R/R$  towards *S. aureus* at  $10^5$  CFU mL $^{-1}$ .

### Preparation of real samples

Lettuce and shrimp samples were purchased from a local supermarket. Three pieces of fresh lettuce leaves or twenty grams of shrimp meat were firstly chopped and dispersed in 200 mL 1  $\times$  PBS (pH 7.4) for homogenization. The supernatant was then filtered through a 0.22- $\mu$ m-pore-size membrane filter (Millipore), and the filtrate was spiked with a known amount of *S. aureus* to a desired concentration. The pretreated samples were analyzed using the proposed assay.

## Results and discussion

### Monomer selection and comparison

The choice of functional monomer determines the success of molecular imprinting and the recognition ability of MIPs to a large extent.<sup>44</sup> Here, TAA, TBA, TMA, and TE were selected as functional monomers for BIF preparation by considering the presence of special functional groups including carboxyl, boric acid, amino, and hydroxyl groups, which may interact with the bacterial surface through hydrogen bonding. To verify if all four monomers were suitable for bacteria imprinting, EIS was carried out to monitor the impedance change during the steps of electro-copolymerization of the template (*S. aureus*) and the monomer, and template elution. As shown in Fig. S1A–D,<sup>†</sup> the impedance values of each electropolymerized film formed in the presence of *S. aureus* were much larger than those of films fabricated in the absence of the template. After elution, the impedance of each BIF decreased significantly. These results suggested that these four 3-substituted thiophene monomers can achieve the success of bacteria imprinting. To investigate their recognition capability, the EIS spectra of the four different BIFs and NIFs towards the target *S. aureus* ( $10^5$  CFU mL $^{-1}$ ) were recorded. The results are shown in Fig. S1E–H.<sup>†</sup> The corresponding EIS responses (bar charts) are shown in Fig. 1 (left coordinate axis). Furthermore, the imprinting effect was evaluated in terms of the imprinting factor (IF), which was calculated according to the ratio of  $\Delta R/R$  for *S. aureus* detected on the BIF compared to that on the NIF.<sup>24</sup> The BIF with amino groups exhibited a strong non-specific adsorption, giving the lowest IF value (1.62), while the BIF with hydroxyl groups produced the highest IF value (4.98), which would help improve the selectivity and sensitivity of the sensor. Therefore, TE was eventually employed as the monomer for the BIF preparation in the following experiment. The above results confirmed the importance of functional groups on the recognition performance of MIPs.<sup>39,45</sup> In this case, we may speculate that the specific recognition of bacteria-imprinted polymer for pathogenic bacteria could be improved by regulating the functional groups of the polymer.

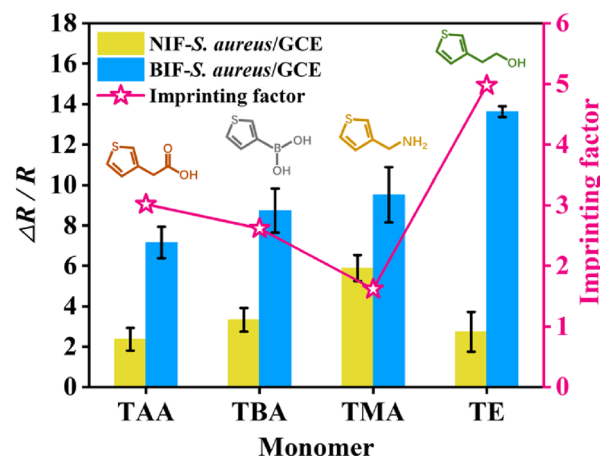


Fig. 1 EIS response towards target *S. aureus* ( $10^5$  CFU mL $^{-1}$ ) with each BIF and NIF prepared using different 3-substituted thiophene monomers (bar chart), and the corresponding imprinting factor (line chart).

### Electrochemical and fluorescent characterization of bacterial imprinting and recognition

The process of bacterial imprinting and recognition using TE as the monomer was characterized by EIS and CV techniques. Fig. 2A and B show the EIS Nyquist plots of differently modified GCEs. It is known that the impedance spectrum includes a linear part and a semicircle portion corresponding to diffusion and electron-limited processes, respectively.<sup>46</sup> The semicircle diameter equals the charge-transfer resistance ( $R_{ct}$ ) through the fitting of the Nyquist plots using the Randles equivalent circuit (inset of Fig. 2A).<sup>47</sup> The bare GCE exhibited almost a straight line (Fig. 2A, solid square), indicating an excellent electron transfer rate on the electrode surface. After the electro-copolymerization of the TE monomer and *S. aureus* template on the bare GCE (PTE + *S. aureus*/GCE), a large semicircle domain was observed (Fig. 2A, solid circle). In comparison, a very tiny semicircle domain was found when the electro-polymerization was performed on the TE monomer alone (PTE/GCE, Fig. 2B, solid square). The result indicated that the template bacteria were successfully doped in the PTE matrices. On immersing the modified electrode (PTE + *S. aureus*/GCE) in CTAB/Hac for 10 min, the semicircle domain of the formed BIF/GCE (Fig. 2A, hollow circle) decreased significantly, suggesting that the template bacteria were successfully removed from the PTE matrices. Upon the capture of *S. aureus* ( $10^5$  CFU mL $^{-1}$ ) using the as-prepared BIF/GCE for 10 min, the semicircle domain of the modified electrode (BIF-*S. aureus*/GCE, Fig. 2A, solid triangle) increased obviously. The calculated  $R_{ct}$  value of the BIF-*S. aureus*/GCE (ca. 3.5 k $\Omega$ ) was 16 times more than that of the BIF/GCE (ca. 210  $\Omega$ ). In contrast, the impedance of NIF-*S. aureus*/GCE (Fig. 2B, hollow circle) was just a little bit higher than that of NIF/GCE (Fig. 2B, solid triangle), signifying a negligible non-specific adsorption of the imprinted film. The result initially revealed that the formed BIF had good recognition capability toward the target *S. aureus*.

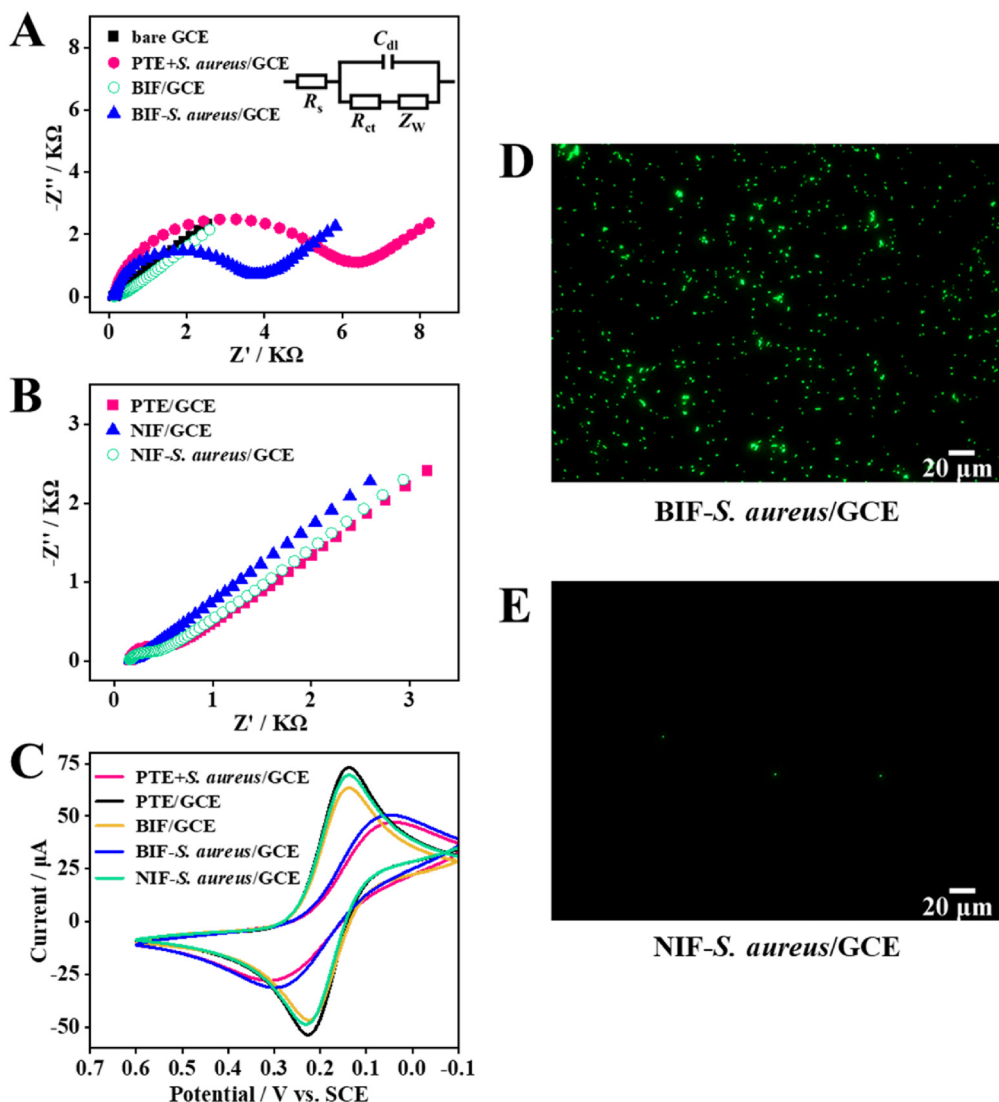


Fig. 2 (A) and (B) EIS and (C) CV curves of differently modified GCEs as indicated. (D) and (E) Fluorescence images showing the recognition of the BIF/GCE and NIF/GCE towards stained *S. aureus* ( $10^5$  CFU  $\text{mL}^{-1}$ ) by green SYTO 9 dye. The inset in (A) is the equivalent circuit model, where  $R_s$ ,  $C_{dl}$ , and  $Z_w$  represent solution resistance, double-layer capacitance, and Warburg impedance, respectively.

The findings mentioned above were confirmed by CV analysis. As shown in Fig. 2C, the CV curve of the PTE + *S. aureus*/GCE exhibited a significant increase in peak potential difference ( $\Delta E_p$ ) and a noticeable decrease in the peak current ( $I_p$ ) compared with that of PTE/GCE. This result confirmed the successful embedding of *S. aureus* in the PTE matrices. After elution, the CV curve of the BIF/GCE showed a similar shape as that of the PTE/GCE, further revealing the complete removal of *S. aureus* from the PTE matrices. After the recognition of *S. aureus*, the CV curve of the BIF-*S. aureus*/GCE had a remarkable change with a rise in  $\Delta E_p$  and a reduction in  $I_p$ , compared with the BIF/GCE and NIF-*S. aureus*/GCE. The result again indicated that the BIF had good recognition capability toward the template bacteria with almost no non-specific adsorption.

To visualize the recognition ability of the imprinted film, the target *S. aureus* was stained with a green fluorescent SYTO

9 dye that is a cell-permeating nucleic acid stain. After incubation, many green spherical spots were found on the surface of the BIF/GCE (Fig. 2D), while almost no fluorescent signals could be found on the NIF/GCE (Fig. 2E). The above results further demonstrated that the BIF had good recognition capability toward the template *S. aureus*.

#### Morphological characterization

The surface morphology of the electrode during bacterial imprinting and recognition were characterized by scanning electron microscopy (SEM, JSM-7800F, JEOL, Japan) and atomic force microscopy (AFM, Bruker Corp., USA). A lot of spherical bacteria were seen on the PTE + *S. aureus*/GCE (Fig. 3A). Most of the bacteria adhered to each other, looking like the shape of grapes with a diameter of *ca.* 0.7  $\mu\text{m}$ , which is consistent with the published literature.<sup>48,49</sup> The result again

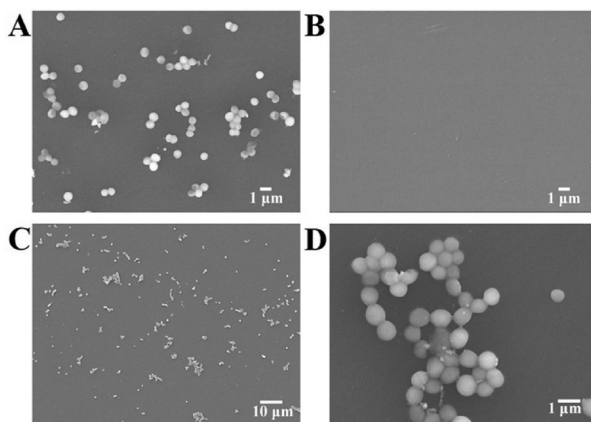


Fig. 3 SEM images of differently modified GCEs: (A) PTE + *S. aureus*/GCE, (B) BIF/GCE, (C) and (D) BIF-*S. aureus*/GCE with 1000-, and 10 000-fold magnification, respectively.

implied that *S. aureus* was successfully doped on the PTE matrices. After elution, no more bacteria were left on the BIF/GCE (Fig. 3B), further suggesting that *S. aureus* was wholly removed. Similar phenomena were observed from AFM images (Fig. S2†). Using the BIF/GCE as the capture electrode, many spherical bacteria were observed on BIF-*S. aureus*/GCE within just 10 min (Fig. 3C), which could be more clearly seen from the magnified image as shown in Fig. 3D.

### Optimization of the BIF-based sensing performance

To optimize the performance of the BIF-based impedimetric sensor, a series of experimental parameters employed in the BIF preparation and the bacteria recognition were systematically optimized. With the increase of the polymerization cycle from 5 to 15 (Fig. 4A), the EIS response first changed little and then decreased obviously due to the increased difficulty in template removal when a thicker polymer film was formed. Thus 10 cycles of polymerization were employed for the BIF fabrication. With the increase of the *S. aureus* template amount from  $10^7$  to  $10^9$  CFU mL $^{-1}$  (Fig. 4B), the EIS response increased gradually due to the formation of more recognition sites. Therefore,  $10^9$  CFU mL $^{-1}$  of *S. aureus* was applied for the BIF preparation.

For the complete removal of a large bacterial template from PTE matrices, we first adopted two existing elution methods, including the successive use of lysozyme (10 mg mL $^{-1}$ ) for 2 h and Triton X-100 (10%) for 80 min (denoted as lysozyme + Triton), and the use of SDS/HAc (5%, w/v) for 4 h. However, the template removal was not complete with a slight decrease of the impedance value. For a more efficient elution, a cationic detergent, CTAB, often used in bacterial lysis,<sup>50</sup> was attempted for the bacterial template removal and compared with the two eluents above. As shown in Fig. 4C, the best elution effect was achieved with CTAB/HAc. In addition, the elution time with CTAB/HAc was also optimized (Fig. 4D). With the increase in the elution time from 5 to 15 min, the  $R_{ct}$  value of the modified electrode first decreased and then changed little.

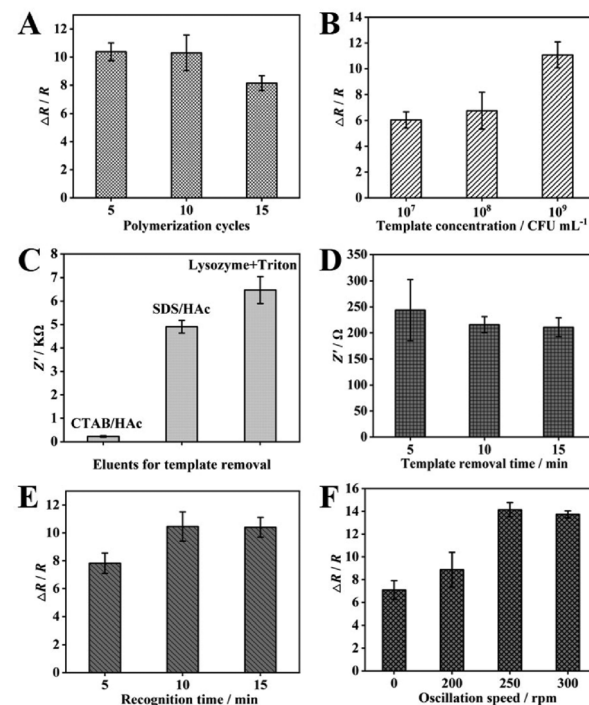


Fig. 4 Optimization of experimental conditions for the BIF preparation and its recognition: (A) polymerization cycles, (B) template concentration, (C) eluents used for template removal, (D) template removal time, (E) recognition time, and (F) oscillation speed during recognition.

Therefore, 10 min of elution with CTAB/HAc was finally used for the bacterial template removal.

To maximize the EIS response toward the target *S. aureus*, the recognition time and oscillation speed during recognition were also optimized. With the increase in the recognition time from 5 to 15 min, the EIS response was enhanced and then changed little (Fig. 4E). Hence, 10 min of recognition was used in the subsequent experiment. Oscillation using a metal bath was employed for *S. aureus* capture to prevent bacterial deposition. With an increase of the oscillation speed from 0 to 300 rpm, the EIS response first increased and then decreased (Fig. 4F). Therefore, 250 rpm was selected for *S. aureus* recognition.

### Quantitative detection of *S. aureus*

With an increase of concentration from 0 to  $10^7$  CFU mL $^{-1}$ , the impedance of BIF/GCE gradually increased (Fig. 5A). This is because the more bacteria are rebound to the BIF, the more imprinted sites are occupied, which reduces the electron transfer between the  $[\text{Fe}(\text{CN})_6]^{3-/-4-}$  redox probe and GCE. Meanwhile, in a broad concentration ranging from  $10^1$  to  $10^7$  CFU mL $^{-1}$ , the EIS response had an excellent linear relationship with the logarithm of the *S. aureus* concentration (Fig. 5B). The linear regression equation for this sensor was expressed as  $\Delta R/R(\Omega) = 2.39 \lg C_{S. aureus} + 0.62$  with a correlation coefficient ( $R^2$ ) of 0.995. Based on the  $3\sigma/S$  rule ( $\sigma$  is the standard deviation of the EIS response for the blank solution,

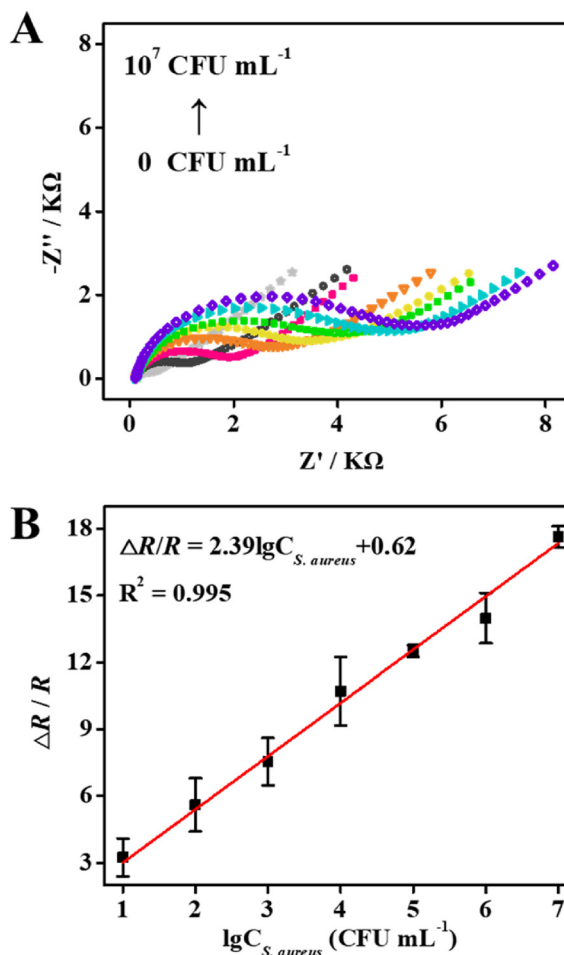


**Fig. 5** (A) EIS of the BIF-based sensor for the detection of *S. aureus* at a series of gradient concentrations from 0 to  $10^7$  CFU  $\text{mL}^{-1}$ . (B) Corresponding calibration curve of the EIS response versus the logarithm of *S. aureus* concentration.

and  $S$  represents the slope of the calibration curve,<sup>49</sup> the detection limit of the sensor was calculated to be 4 CFU  $\text{mL}^{-1}$ , which was comparable to or even better than other reported label-free electrochemical sensors for *S. aureus* detection as shown in Table S1.†

#### Selectivity and universality of the BIF-based sensor

The selectivity was firstly investigated by comparing the EIS response of *S. aureus*-templated BIF to single bacteria (the target or interfering bacteria), and bacterial mixture with or without *S. aureus*. As shown in Fig. 6A, the EIS response of *S. aureus*-templated BIF towards the target *S. aureus* was 5 times higher than that to the interfering bacteria (*E. coli* O157, *S. paratyphi* B, or *L. monocytogenes*). Moreover, the EIS response of *S. aureus*-templated BIF to the bacterial mixtures with *S. aureus* was approximately 4 times larger than that without *S. aureus*. This result revealed that the selectivity of this sensor is excellent. The high selectivity of the BIF against

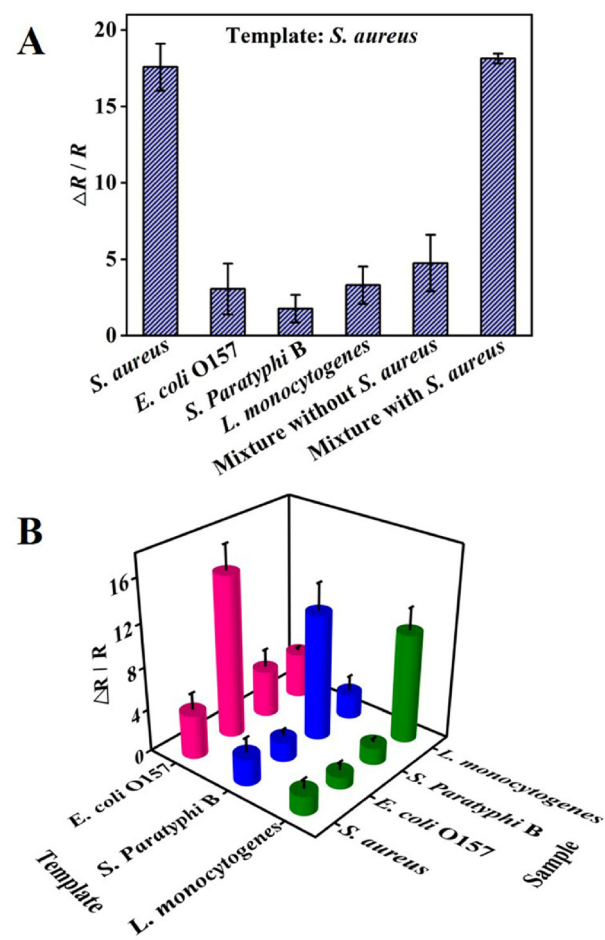


**Fig. 6** Selectivity and universality of the BIF-based sensor. (A) EIS response of *S. aureus*-templated BIF to single bacteria, and multi-bacterial strain mixtures without (mixture A) and with *S. aureus* (mixture B). (B) EIS response of *E. coli* O157-, *S. Paratyphi* B-, and *L. monocytogenes*-templated BIF to the target bacteria and interfering bacteria. Each type of bacteria was maintained at the same concentration of  $10^5$  CFU  $\text{mL}^{-1}$ .

the template bacteria could be ascribed to its sensitivity to the chemical conformation of bacterial outer cell structures.<sup>37</sup>

To test whether this BIF-based sensor can be applied for detecting other bacteria, three other bacteria, including *E. coli* O157, *S. paratyphi* B, and *L. monocytogenes*, were individually used as the template for BIF preparation. It was found that for each *E. coli* O157-, *S. paratyphi* B-, or *L. monocytogenes*-templated BIF, the EIS response to the corresponding template bacteria was at least 3 times more than that to the interfering bacteria (Fig. 6B). The above results showed that the BIF-based sensor could provide a universal method for the highly selective detection of bacterial pathogens.

#### Reusability and repeatability of the sensing interface

The imprinted sites after the bacterial rebinding could be efficiently regenerated within 10 min using the same method as the template removal. It can be seen that even after being

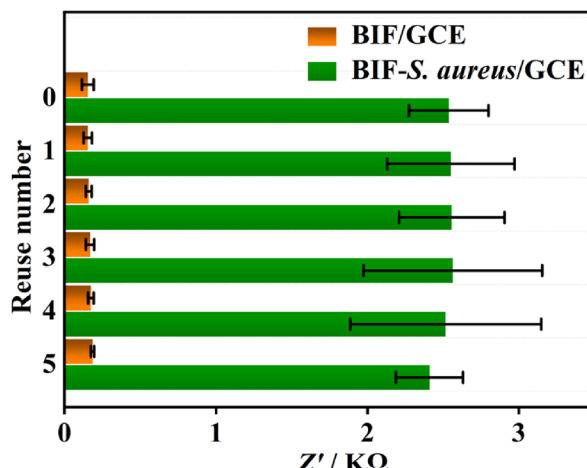


**Fig. 7** Reusability of the BIF-based sensing interface. The impedance of BIF/GCE before and after the recognition of *S. aureus* ( $10^5$  CFU mL $^{-1}$ ) with different reuse numbers.

recycled 5 times, the impedance response to the target *S. aureus* still retained more than 90% of the initial detection signal (Fig. 7). The result indicated that the BIF-based sensor is reusable, which is meaningful for reducing the assay cost and time.

The repeatability was tested by monitoring the EIS responses of eight fabricated BIF/GCE electrodes toward *S. aureus* ( $10^5$  CFU mL $^{-1}$ ) in 0.01 M PBS (pH 7.4). It was found that the relative standard deviation % (RSD %) did not exceed 4.2%, indicating the good repeatability of the BIF-based sensor.

#### Detection of *S. aureus* in real samples

To demonstrate the practical application of the proposed BIF-based sensor for *S. aureus* detection in real complex samples, we have used it for the analysis of lettuce and shrimp samples artificially contaminated with different concentrations of *S. aureus*. As can be seen from Table 1, the average recoveries of *S. aureus* vary from 92.9 to 110.6%. The results implied that the BIF-based sensor had a promising potential for the determination of bacteria in real samples. The sensing strategy

**Table 1** Detection of *S. aureus* in lettuce and shrimp samples

Sample	Amounts of <i>S. aureus</i> (CFU mL $^{-1}$ )		
	Added	Measured	Recovery (%)
Lettuce	$10^1$	$10.40 \pm 1.1$	104.0
	$10^2$	$108.0 \pm 24.3$	108.0
	$10^3$	$929.1 \pm 292.4$	92.9
Shrimp	$10^2$	$102.5 \pm 27.7$	102.5
	$10^3$	$1106.0 \pm 261.1$	110.6
	$10^4$	$9922.0 \pm 557.2$	99.2

All data are represented as the average value  $\pm$  standard deviation of at least three independent experiments.

could also be extended to on-site, remote, or home monitoring of bacterial pathogens through combining disposable electrodes (e.g., screen-printed electrodes, carbon paper, etc.) and commercial portable electrochemical workstations.

## Conclusion

In summary, an efficient label-free impedimetric sensing strategy based on an electropolymerized BIF has been developed for the rapid and sensitive detection of *S. aureus*. The results suggest that the specific recognition of MIPs can be modulated by designing suitable functional groups. In contrast to most reported label-free electrochemical sensors for *S. aureus* detection (Table S1†), a significant improvement on both the duration for sensing interface fabrication and the analysis time was achieved with a comparable detection limit. Moreover, the BIF sensing interface can be regenerated and reused up to five times, which is effective in reducing the assay cost and time. This assay is anticipated to provide a universal, simple, and robust method for the rapid, sensitive, and low-cost detection of pathogenic bacteria. Yet, there are still challenges in identifying live/dead bacteria, detecting complex food or whole blood samples without complicated sample pretreatment, and achieving long-term stability.

## Author contributions

Lingling Wang: conceptualization, investigation. Xiaohui Lin: conceptualization, writing – original draft. Ting Liu: investigation. Zhaohuan Zhang: methodology. Jie Kong: data curation. Hai Yu: investigation. Juan Yan: visualization and investigation. Donglei Luan: investigation. Yong Zhao: supervision and funding acquisition. Xiaojun Bian: conceptualization, supervision, methodology, writing – review and editing, and project administration.

## Conflicts of interest

There are no conflicts to declare.

## Acknowledgements

We gratefully acknowledge financial support from the Program of Shanghai Academic Research Leader (21XD1401200), the Agricultural Project of Shanghai Science and Technology Innovation Action Plan (19391901600), the Natural Science Foundation of Shanghai Municipal (20ZR1424100, 20ZR1423800), and Chengguang Program supported by the Shanghai Education Development Foundation and the Shanghai Municipal Education Commission (15CG54).

## References

1 C. S. Ho, N. Jean, C. A. Hogan, L. Blackmon, S. S. Jeffrey, M. Holodniy, N. Banaei, A. A. E. Saleh, S. Ermon and J. Dionne, *Nat. Commun.*, 2019, **10**, 4927.

2 P. N. Reddy, K. Srirama and V. R. Dirisala, *Infect. Dis.*, 2017, **10**, 1179916117703999.

3 W. Kong, J. Xiong, H. Yue and Z. Fu, *Anal. Chem.*, 2015, **87**, 9864–9868.

4 W. C. Hu, J. Pang, S. Biswas, K. Wang, C. Wang and X. H. Xia, *Anal. Chem.*, 2021, **93**, 8544–8552.

5 M. M. Ali, R. Silva, D. White, S. Mohammadi, Y. Li, A. Capretta and J. D. Brennan, *Angew. Chem.*, 2022, **61**, e202112346.

6 V. Fabre, K. C. Carroll and S. E. Cosgrove, *J. Clin. Microbiol.*, 2022, **60**, e01005–e01021.

7 Y. Cui, H. Wang, F. Guo, X. Cao, X. Wang, X. Zeng, G. Cui, J. Lin and F. Xu, *Food Chem.*, 2022, **391**, 133241.

8 W. Yin, L. Zhu, H. Xa, Q. Tang, Y. Ma, S.-H. Chou and J. He, *Sens. Actuators, B*, 2022, **366**, 132005.

9 P. Athamanolap, K. Hsieh, C. M. O'Keefe, Y. Zhang, S. Yang and T.-H. Wang, *Anal. Chem.*, 2019, **91**, 12784–12792.

10 B. Wu, J. S. Hu and Y. Li, *Food Microbiol.*, 2022, **106**, 104052.

11 J. Yi, X. Wang, Y. Dai, L. Qiao and B. Liu, *Anal. Chem.*, 2019, **91**, 14220–14225.

12 Z. Chai and H. Bi, *Food Chem.: X*, 2022, **13**, 100225.

13 H. Shengbin, H. Xinyi, Z. Miaomiao, W. Lina and Y. Xiaomei, *Anal. Chem.*, 2020, **92**, 2393–2400.

14 T. Tian, J. Yi, Y. Liu, B. Li, Y. Liu, L. Qiao, K. Zhang and B. Liu, *Biosens. Bioelectron.*, 2022, **197**, 113778.

15 E. Rho, M. Kim, S. H. Cho, B. Choi, H. Park, H. Jang, Y. S. Jung and S. Jo, *Biosens. Bioelectron.*, 2022, **202**, 113991.

16 O. Simoska and K. J. Stevenson, *Analyst*, 2019, **144**, 6461–6478.

17 N. Amin, A. S. Torralba, R. Alvarez-Diduk, A. Afkhami and A. Merkoci, *Anal. Chem.*, 2020, **92**, 4209–4216.

18 F. Zhu, X. Bian, H. Zhang, Y. Wen, Q. Chen, Y. Yan, L. Li, G. Liu and J. Yan, *Biosens. Bioelectron.*, 2021, **176**, 112943.

19 S. B. Somvanshi, A. M. Ulloa, M. Zhao, Q. Liang, A. K. Barui, A. Lucas, K. M. Jadhav, J. P. Allebach and L. A. Stanciu, *Biosens. Bioelectron.*, 2022, **207**, 114214.

20 Y. Wei, Z. Tao, L. Wan, C. Zong, J. Wu, X. Tan, B. Wang, Z. Guo, L. Zhang, H. Yuan, P. Wang, Z. Yang and Y. Wan, *Biosens. Bioelectron.*, 2022, **211**, 114282.

21 E. Fan, J. Peng, Y. He, Y. Wu, H. Ouyang, Z. Xu and Z. Fu, *Sens. Actuators, B*, 2019, **285**, 271–276.

22 M. Amiri, A. Bezaatpour, H. Jafari, R. Boukherroub and S. Szunerits, *ACS Sens.*, 2018, **3**, 1069–1086.

23 L. Chen, X. Wang, W. Lu, X. Wu and J. Li, *Chem. Soc. Rev.*, 2016, **45**, 2137–2211.

24 R. Xing, Y. Wen, Y. Dong, Y. Wang, Q. Zhang and Z. Liu, *Anal. Chem.*, 2019, **91**, 9993–10000.

25 G. Dykstra, B. Reynolds, R. Smith, K. Zhou and Y. Liu, *ACS Appl. Mater. Interfaces*, 2022, **14**, 25972–25983.

26 X. Wang, Y. Liu, J. Liu, J. Qu, J. Huang, R. Tan, Y. Yu, J. Wu, J. Yang, Y. Li, H. Qu and J. Liu, *Biosens. Bioelectron.*, 2022, **208**, 114233.

27 P.-W. Gao, Y.-Z. Shen, C. Ma, Q. Xu and X.-Y. Hu, *Analyst*, 2021, **146**, 6178–6186.

28 P. Li, J. Pang, S. Xu, H. He, Y. Ma and Z. Liu, *Angew. Chem.*, 2022, **61**, e202113528.

29 V. Ratautaite, R. Boguzaite, E. Brazys, A. Ramanaviciene, E. Ciplys, M. Juozapaitis, R. Slibinskas, M. Bechelany and A. Ramanavicius, *Electrochim. Acta*, 2022, **403**, 139581.

30 L. Luo, F. Zhang, C. Chen and C. Cai, *Anal. Chem.*, 2019, **91**, 15748–15756.

31 Z. Zhang, Y. Guan, M. Li, A. Zhao, J. Ren and X. Qu, *Chem. Sci.*, 2015, **6**, 2822–2826.

32 B. Tse Sum Bui, T. Auroy and K. Haupt, *Angew. Chem.*, 2022, **61**, e202106493.

33 N. Idil, M. Hedstrom, A. Denizli and B. Mattiasson, *Biosens. Bioelectron.*, 2017, **87**, 807–815.

34 X. Shen, J. Svensson Bonde, T. Kamra, L. Bulow, J. C. Leo, D. Linke and L. Ye, *Angew. Chem., Int. Ed.*, 2014, **53**, 10687–10690.

35 J. Borovicka, W. J. Metheringham, L. A. Madden, C. D. Walton, S. D. Stoyanov and V. N. Paunov, *J. Am. Chem. Soc.*, 2013, **135**, 5282–5285.

36 J. Niu, L. Wang, T. Cui, Z. Wang, C. Zhao, J. Ren and X. Qu, *ACS Nano*, 2021, **15**, 15841–15849.

37 S. Tokonami, Y. Nakadoi, M. Takahashi, M. Ikemizu, T. Kadoma, K. Saimatsu, Q. Dung le, H. Shiigi and T. Nagaoka, *Anal. Chem.*, 2013, **85**, 4925–4929.

38 L. M. Gonçalves, *Curr. Opin. Electrochem.*, 2021, **25**, 100640.

39 J. Pan, W. Chen, Y. Ma and G. Pan, *Chem. Soc. Rev.*, 2018, **47**, 5574–5587.

40 S. Ramanavicius and A. Ramanavicius, *Adv. Colloid Interface Sci.*, 2022, **305**, 102693.

41 J. Zhang, Y. Wang and X. Lu, *Anal. Bioanal. Chem.*, 2021, **413**, 4581–4598.

42 W. Jiang, A. Saxena, B. Song, B. B. Ward, T. J. Beveridge and S. C. B. Myneni, *Langmuir*, 2004, **20**, 11433–11442.

43 M. Golabi, F. Kuralay, E. W. Jager, V. Beni and A. P. Turner, *Biosens. Bioelectron.*, 2017, **93**, 87–93.

44 A. G. Ayankojo, A. Tretjakov, J. Reut, R. Boroznjak, A. Opik, J. Rappich, A. Furchner, K. Hinrichs and V. Syritski, *Anal. Chem.*, 2016, **88**, 1476–1484.

45 K. R. a. R. N. Zare, *ACS Nano*, 2012, **6**, 4314–4318.

46 S. Dong, R. Zhao, J. Zhu, X. Lu, Y. Li, S. Qiu, L. Jia, X. Jiao, S. Song, C. Fan, R. Hao and H. Song, *ACS Appl. Mater. Interfaces*, 2015, **7**, 8834–8842.

47 A. Ahmed, J. V. Rushworth, N. A. Hirst and P. A. Millner, *Clin. Microbiol. Rev.*, 2014, **27**, 631–646.

48 F. Yang, T. L. Chang, T. Liu, D. Wu, H. Du, J. Liang and F. Tian, *Biosens. Bioelectron.*, 2019, **133**, 147–153.

49 R. Wang, L. Wang, J. Yan, D. Luan, S. Tao, J. Wu and X. Bian, *Talanta*, 2021, **226**, 122135.

50 G. C. Allen, M. A. Flores-Vergara, S. Krasynanski, S. Kumar and W. F. Thompson, *Nat. Protoc.*, 2006, **1**, 2320–2325.